Sub-pixel Edge Detection Algorithm Using Dynamic PCA-Hessian Method

Wang Shibo[1], Wang Yan[1,3*], Li Wenhui[1,3*], Yin Xiaoming[1,3], Xu Min[1,3], Zheng Zhongpeng[1,3], and Xie GuiJiu[2]

[1]College of Mechanical Engineering, Tianjin University of Science and Technology, Tianjin, China
[2]College of Mechanical Engineering, University of Science and Technology Beijing, Beijing, China
[3]Tianjin Key Laboratory of Integrated Design and Online Monitoring of Light Industry and Food Engineering Machinery Equipment, Tianjin, China
E-mail : satansdestiny@163.com
*Corresponding author
Manuscript received May 2, 2026; accepted May 15, 2026; published June 15, 2026

***Abstract*—To address the issue of insufficient localization accuracy in traditional edge detection methods applied to the complex texture background of the flame-retardant composite material A500H11, this study proposes a high-precision subpixel edge detection and line connection optimization algorithm. Building upon the Steger algorithm, this method introduces a Sigmoid function to adaptively adjust the analysis window based on local gradient magnitudes. It combines the noise suppression capability of Principal Component Analysis with the directional advantage of the Hessian matrix to achieve dynamic hybrid correction of subpixel coordinates. To further enhance edge continuity and integrity, a multi-strategy post-processing workflow is designed, incorporating neighborhood constraints, dynamic programming for path optimization, and B-spline interpolation. Experimental results demonstrate that the average displacement error and standard deviation of the proposed algorithm for scratches and cracks are both below 0.3 pixels, with the proportion of high-precision points exceeding 80%. Compared with morphological post-processing methods, the edge continuity index is improved by an average of 69.6%, and the contour integrity score is enhanced by an average of 15.5%. This method effectively overcomes complex texture interference, achieving high-precision and high-continuity subpixel edge extraction, thereby providing a viable solution for visual inspection under low-contrast and high-texture background conditions.**

***Keywords*—Edge detection; Sub-pixel positioning; PCA; Hessian matrix; Post-processing optimization**

I. INTRODUCTION

The risk of fire and explosion associated with new energy batteries is one of the critical challenges in the rapid development of the new energy sector. The flame-retardant composite material A500H11, owing to its excellent fireproof and thermal insulation properties, is widely used in safety protection components such as battery pack top covers. However, the surface of this material exhibits complex textural backgrounds, and typical defects such as scratches and cracks are characterized by low contrast and weak edges, imposing high demands on the accuracy and robustness of detection algorithms [1, 2]. As the foundation for subsequent measurements of width, length, and area, the localization accuracy of defect edges directly affects the reliability of quality assessment [3, 4]. Therefore, researching algorithms capable of achieving high-precision and high-continuity edge extraction under complex textured backgrounds holds significant theoretical importance and engineering application value.

Existing subpixel edge detection methods mainly include moment-based methods, gradient-based methods, and learning-based methods. Moment-based methods utilize the statistical properties of image grayscale distribution for edge localization, offering strong noise resistance and high localization accuracy. Du *et al.* [5] proposed a subpixel edge detection method integrating Franklin moments, which compresses the runtime to 66% of that of the Canny-Zernike moment method while maintaining accuracy. Guo *et al.* [6] combined an improved Canny adaptive threshold with a novel Zernike edge judgment criterion, significantly reducing the relative error in flange dimension measurement. However, these methods exhibit insufficient response to weak edges under complex textured backgrounds, resulting in limited localization stability on materials such as A500H11.

Gradient-based methods determine edge positions by solving image derivatives, offering high computational efficiency and ease of implementation. Jie *et al.* [7] integrated improved adaptive Canny edge detection with subpixel contour fitting to achieve submicron repeatability precision in Z-block precision positioning. Cheng *et al.* [8] employed Canny-Steger subpixel edge detection for visual measurement of shaft parts, achieving a 60% improvement in accuracy compared to pixel-level methods. However, traditional gradient methods are sensitive to noise and prone to localization or edge fractures in weak edge regions, making it difficult to balance accuracy and continuity.

In recent years, learning-based methods have demonstrated strong potential in edge detection tasks. Xu *et al.*[9] proposed a markerless wide-field optical measurement method integrating subpixel edge detection, residual correction, and transfer learning, achieving displacement measurement errors of less than 1 mm at a distance of 100 meters. Wang *et al.* [10] combined lightweight YOLOv8 with subpixel edge detection to achieve high-precision measurement of elevator traction sheave groove wear, with a maximum absolute error of only 0.062 mm. However, deep learning methods rely on large-scale annotated data, and their generalization capability in industrial scenarios with complex textures and weak defects remains to be validated.

In summary, existing methods still face challenges when processing materials with complex textured backgrounds such as A500H11. This paper proposes a high-precision Steger subpixel edge detection and line connection optimization algorithm. A Sigmoid function is introduced to adaptively adjust the analysis window, and the noise suppression capability of PCA is leveraged to achieve

accurate correction of subpixel coordinates. A multi-strategy fusion line connection and pipeline is designed, incorporating neighborhood connection, dynamic programming path optimization, and B-spline curve interpolation repair, significantly enhancing edge continuity and integrity. This provides an effective solution for high-precision visual detection under complex textured backgrounds.

II. Dynamic Hybrid PCA-Hessian Sub-pixel Localization

The traditional Steger algorithm, which is based on Hessian matrix eigendecomposition, exhibits poor adaptability in weak edge regions and high sensitivity to noise, significantly limiting its real-time performance and robustness [11-14]. Building upon this foundation, this chapter proposes a dynamic hybrid PCA-Hessian subpixel edge localization algorithm. While maintaining subpixel-level positioning accuracy, this method substantially enhances the algorithm's adaptability under complex textured backgrounds. The specific steps are as follows:

A. Improved Steger Sub-pixel Edge Localization

To balance localization accuracy and noise suppression capability, a Sigmoid function is introduced to adaptively select the analysis window size based on local gradient magnitude. In strong edge regions, a small window is employed for rapid Hessian matrix computation to achieve fast and precise localization. In weak edge regions, a large window is utilized to suppress noise through PCA statistics, thereby improving the detection rate of weak edges.

The standard Sigmoid function is shifted and scaled by introducing a gradient magnitude threshold T to control the central position of the window size W variation, shifting the center point to T, where k serves as the steepness coefficient controlling the transition rate. Meanwhile, the output range is mapped from (0,1) to ($W_{\min}$,$W_{\max}$). The improved Sigmoid function takes the following form:

$$W(M)=W_{\min}+\frac{W_{\max}-W_{\min}}{1+e^{-k(M_{norm}-T)}} \tag{1}$$

In the equation, M_{norm} represents the normalized local gradient magnitude, while $W_{\min}$ and $W_{\max}$ denote the minimum and maximum window sizes, respectively. When M_{norm}=T, the derivative of the function reaches its maximum, resulting in the fastest change in window size, thereby achieving adaptive transition.

To achieve accurate estimation of the normal direction, this paper dynamically combines the advantages of both the Hessian matrix and PCA. The direction angle cosines n_{H} and n_{P} are computed separately, followed by direction correction to ensure directional consistency between the two methods.

$$cos\theta=n_H\cdot n_P=n_{Hx}n_{Px}+n_{Hy}n_{Py} \tag{2}$$

Furthermore, a hybrid weighting function is designed to dynamically adjust the contribution weights of the Hessian matrix and PCA based on the gradient magnitude M. In strong edge regions, the Hessian matrix is primarily utilized, while PCA dominates in weak edge regions. A smooth transition is achieved through the gradient magnitude weighting function W(M):

$$n_{hybrid}=W(M)\cdot n_H+(1-W(M))\cdot n_p \tag{3}$$

In the equation, $W(M)$ adopts a Sigmoid form similar to Equation 1, ensuring a continuous transition of the hybrid direction between strong and weak edge regions. The final hybrid direction n_{hybrid} is subsequently normalized.

Taylor expansion is performed along this normal direction to solve for the subpixel-level offset, achieving precise localization beyond the limitations of the pixel grid [15]. In strong edge regions, the second-order derivative is directly computed using the Hessian matrix, whereas in weak edge regions, it is approximated using the gradient difference method via PCA.

$$\frac{\partial^2 I}{\partial t^2}=n^T Hn=I_{xx}n_x^2+2I_{xy}n_xn_y+I_{yy}n_y^2 \tag{4}$$

$$\frac{\partial^2 I}{\partial t^2}\approx\frac{G_x(x+\Delta n_x,y+\Delta n_y)-G_x(x,y)}{\Delta}n_x+\frac{G_y(x+\Delta n_x,y+\Delta n_y)-G_y(x,y)}{\Delta}n_y \tag{5}$$

Performing a second-order Taylor expansion of the gray profile along the normal direction n_{hybrid}, the subpixel offset t is obtained by setting the first derivative to zero.

$$t=-\frac{G_xn_x+G_yn_y}{I_{xx}n_x^2+2I_{xy}n_xn_y+I_{yy}n_y^2} \tag{6}$$

Substituting the offset t into the coordinate parameterization equation yields the corrected subpixel edge coordinates (x_{sub} , y_{sub}):

$$(x_{sub},\ y_{sub})=(x_0+t\cdot n_x,\ y_0+t\cdot n_y) \tag{7}$$

B. Line Connection and Post-Processing Optimization

The subpixel edge points generated by the above steps may exhibit discrete distributions due to noise, uneven illumination, or fractures inherent to the defects themselves [16-18]. To enhance the continuity and integrity of defect edges, this paper designs a post-processing pipeline incorporating neighborhood connection, dynamic programming path optimization, and B-spline curve interpolation repair.

Neighborhood-constrained connection aggregates discrete subpixel edge points as graph nodes, connecting edge points that are spatially proximate and directionally consistent. By integrating spatial distance and directional difference, the edge weight E_{ij} is defined as follows:

$$E_{ij}=\alpha\cdot\frac{\|p_i-p_j\|}{d_{max}}+(1-\alpha)\cdot\left(1-\left|\cos(\theta_i-\theta_j)\right|\right) \tag{8}$$

where P_{i} and P_{j} denote the coordinates of the edge points, θ_{i} and θ_{j} represent their corresponding normal directions, $d_{\max}$ is the maximum connection distance threshold, and α is a balancing coefficient. The smaller the weight, the higher the likelihood of connection between two points.

To address issues such as path branching or directional discontinuity after preliminary connection [19], dynamic programming is employed to further optimize the smoothness and directional continuity of the path. The dynamic programming recurrence equation is established through the local cost function C_{trans} and the transition cost function C_{local}:

$$D(p_i)=\min_{p_j\in P(p_i)}\left[D(p_i)+C_{trans}(p_j,p_i)\right]+C_{local}(p_i), \tag{9}$$

where $P(p_{\text{i}})$ represents the set of predecessor nodes of p_{i}. By recursively backtracking from the end point, the optimal path is obtained, effectively resolving the issue of local

suboptimal choices.

For fractured regions, interpolation repair is performed using cubic B-spline curves, leveraging their local controllability and high-order continuity [20]. This effectively fills the fracture regions while enhancing noise resistance and adaptability. The cubic B-spline curve $Q(u)$ is defined as:

$$Q(u)=\sum_{i=0}^{n} N_{i,3}(u)\cdot q_i, \quad u\in[0,1] \tag{10}$$

where P_i denotes the control points, and $N_i,3(u)$ represents the cubic B-spline basis functions. Parameter u is uniformly sampled within the fracture interval to generate interpolation points, with the corresponding subpixel coordinates given by:

$$(x_k, y_k)=Q(u_k)=\sum_{i=0}^{n} N_{i,3}(u_k)\cdot q_i \tag{11}$$

III. Results and Discussion

To validate the effectiveness of the proposed algorithm, experiments were conducted by acquiring images of four types of surface defects—scratch, crack, fold, and hierarchy—on the modified mica material A500H11 using an industrial camera. The appearance of A500H11 is shown in Fig. 1, and the experimental setup is illustrated in Fig. 2. To verify the improved subpixel localization algorithm proposed in this paper, experimental validation was performed on the Python-OpenCV 3.10 platform, with the experimental environment comprising an Intel Core i7-12700K CPU and 32 GB RAM.

Fig.1. Appearance of the A500H11.

Fig.2. Experimental industrial camera pictures.

A. Experimental Results of Sub-Pixel Positioning Accuracy

To evaluate the accuracy of the proposed dynamic hybrid PCA-Hessian subpixel localization algorithm, gradient-based methods, Zernike moment-based methods, and traditional Steger-based methods were selected as benchmarks. The mean displacement, standard deviation of displacement, and the proportion of high-precision points under different thresholds were adopted as evaluation metrics. A comprehensive rating of algorithm performance was conducted according to the grading criteria shown in Table 1.

Table 1 Comprehensive evaluation level standard for sub-pixel positioning accuracy

Grade	Average displacement	Standard deviation of displacement	Subpixel accuracy rate(<0.5 pixels)	Subpixel accuracy rate(<0.3 pixels)	Subpixel accuracy rate(<0.1 pixels)
Excellent	< 0.3	<0.3	> 80%	> 60%	> 40%
Good	< 0.4	<0.4	> 70%	> 50%	> 20%
Common	< 0.5	<0.6	> 60%	> 40%	> 10%
Bad	> 0.5	> 0.6	< 60%	< 40%	< 10%

As shown in the qualitative analysis in Fig. 3, traditional methods exhibit localization blurring, discrete edge points, or fracture phenomena in weak edge and detail transition regions. In contrast, the edge points obtained by the proposed algorithm are more continuous and smoother, maintaining a dense and precise localization distribution even in complex textured regions.

The quantitative analysis in Table 2 demonstrates that, for scratch defects, the mean displacement of the proposed algorithm is reduced by 48.3%, 61.0%, and 25.7% compared to the gradient-based method, Zernike moment-based method, and Steger-based method, respectively; the standard deviation of displacement is reduced by 23.1%, 37.5%, and 15.8%, respectively; and the accuracy rates for <0.5 pixel, <0.3 pixel, and <0.1 pixel reach 89.17%, 81.29%, and 49.79%, respectively, all significantly outperforming the comparison methods. According to the grading criteria in Table 1, the proposed algorithm achieves an "excellent" rating across all three metrics for scratch localization.

For crack defects, the mean displacement of the proposed algorithm is reduced by 16.9%, 55.0%, and 48.2% compared to the benchmark methods, respectively; the standard deviation of displacement is reduced by 27.6%, 18.2%, and 10.3%, respectively; and the accuracy rates for <0.5 pixel and <0.3 pixel reach 81.91% and 65.93%, respectively, both achieving an "excellent" rating. The <0.1 pixel accuracy rate (38.98%) is slightly below the "excellent" standard (40%). This is attributed to the fact that crack edges are more blurred and exhibit lower contrast compared to scratches, making subpixel localization more challenging. Nevertheless, the experimental results indicate that the proposed algorithm still outperforms the comparison methods on this metric, validating its localization advantage in weak edge regions.

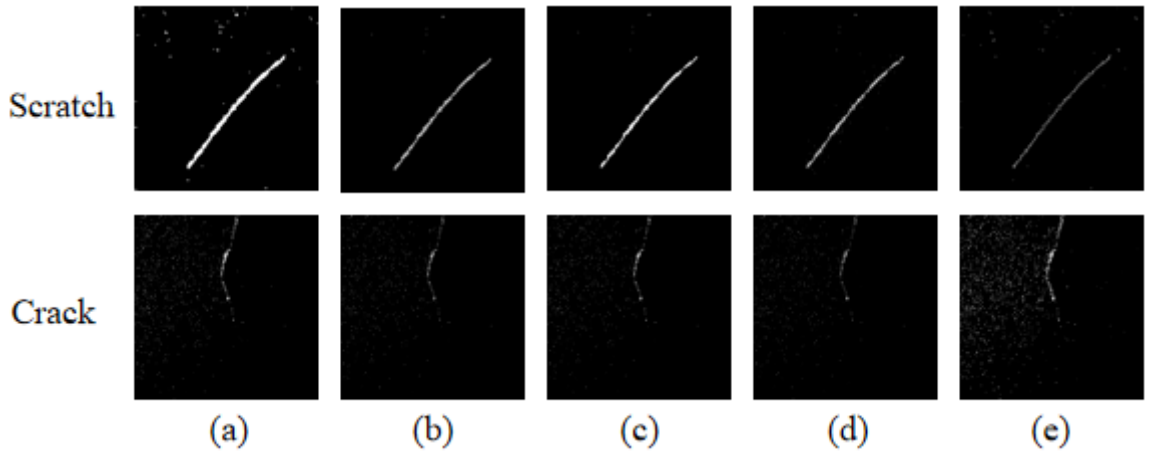

Fig.3. Comparative analysis of A500H11 sub-pixel edge detection effects: (a) Canny edge images; (b) Gradient method; (c) Zernike moment method; (d) Steger method; (e) PCA-Hessian Steger method.

Table 2 Analysis of sub-pixel positioning accuracy

Defect type	Evaluation index	gradient Method	Zernike moment method	Steger method	Improved method
Scratch	Average displacement	0.3517	0.4659	0.2445	0.1817
	Displacement standard deviation	0.3153	0.3878	0.2880	0.2425
	<0.5 pixel accuracy rate	58.26%	52.16%	75.95%	89.17%
	<0.3 pixel accuracy rate	47.05%	31.38%	65.14%	81.29%
	<0.1 pixel accuracy rate	37.94%	11.84%	41.68%	49.79%
Crack	Average displacement	0.2937	0.5426	0.4707	0.2440
	Displacement standard deviation	0.3188	0.2819	0.2573	0.2307
	<0.5 pixel accuracy rate	67.63%	45.63%	75.67%	81.91%
	<0.3 pixel accuracy rate	55.41%	38.44%	63.64%	65.93%
	<0.1 pixel accuracy rate	47.75%	25.12%	43.40%	38.98%

B . Experimental Results of the Line Connection Algorithm

To validate the effectiveness of the proposed multi-strategy post-processing pipeline, three schemes were compared: no connection processing, traditional morphological post-processing, and the complete post-processing pipeline proposed in this paper. Two metrics, the Edge Continuity Index (ECI) and the Contour Integrity Score (CIS), were introduced for quantitative analysis. Specifically, a higher ECI value indicates better edge continuity, while a higher CIS value reflects superior contour integrity.

As shown in Fig. 4, the results without connection processing fail to form meaningful continuous contours. Traditional morphological processing achieves limited connection effectiveness, with noticeable fractures and structural deficiencies still present. In contrast, the proposed algorithm effectively bridges fractured regions, reconstructs the main contour structures, and demonstrates superior capability in preserving continuity and restoring shape.

Table 3 shows that, compared to traditional morphological processing, the proposed algorithm achieves an average improvement of approximately 69.6% in ECI and 15.5% in CIS across all defect types. Specifically, for scratch defects, ECI and CIS are improved by 57.5% and 14.5%, respectively; for crack defects, the most significant improvement is observed, with ECI increased by 99.5% and CIS by 13.5%; for fold defects, ECI and CIS are improved by 65.8% and 7.9%, respectively; and for hierarchy defects, improvements of 55.7% in ECI and 26.1% in CIS are achieved. Experimental results indicate that the proposed algorithm not only enhances edge connection continuity but also better preserves the integrity of contour structures, demonstrating consistent optimization effects across defects of different morphologies.

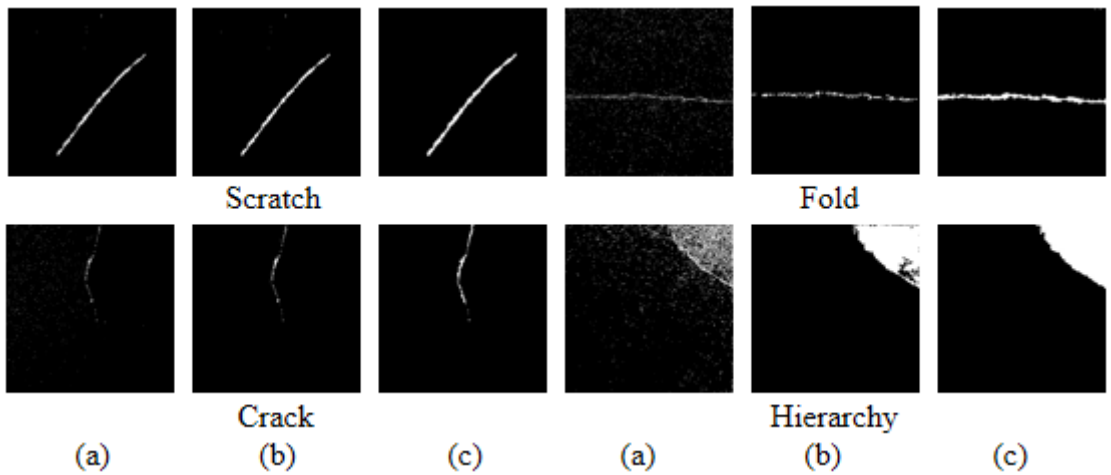

Fig.4. Four defect line connection and post-processing effect diagram: (a) Unprocessed; (b) Traditional morphological; (c) The algorithm of this article.

Table 3 Analysis of line connection and post-processing effects comparison

Defect type	Without connection processing		Traditional morphological processing		Improved post-processing algorithm	
	ECI	CIS	ECI	CIS	ECI	CIS
Scratch	0.4374	0.6148	0.5480	0.7241	0.8632	0.8292
Crack	0.2636	0.3010	0.3470	0.6492	0.6923	0.7369
Fold	0.2528	0.3745	0.3822	0.6745	0.6338	0.7271
Hierarchy	0.2655	0.4673	0.4718	0.5781	0.7347	0.7290

IV. Conclusion

To address the issues of insufficient positioning accuracy and poor edge continuity in traditional edge detection methods under complex textured backgrounds on the surface of the flame-retardant composite material A500H11, this paper proposes a subpixel edge detection and line connection optimization algorithm based on dynamic PCA-Hessian. The main conclusions are as follows. In terms of subpixel localization, the proposed algorithm achieves a mean displacement and standard deviation of displacement below 0.3 pixels for both scratch and crack defects, with the proportion of high-precision points exceeding 80%. It outperforms gradient-based methods, Zernike moment-based methods, and the traditional Steger method in metrics such as mean displacement, standard deviation of displacement, and the proportion of high-precision points, validating its localization advantages in weak edge and complex textured regions. Regarding edge continuity optimization, the proposed algorithm improves the Edge Continuity Index by an average of 69.6% and the Contour Integrity Score by an average of 15.5%, effectively resolving issues of edge fracture and structural distortion under complex textured backgrounds. Although the proposed algorithm achieves satisfactory detection performance under complex textured backgrounds, there remains room for improvement in subpixel localization under extremely weak edge conditions. Future research may further explore the optimization of this algorithm for real-time detection systems and extend its application to visual inspection tasks involving other low-contrast, high-texture background materials.

Conflict of Interest

The authors declare no conflict of interest.

References

[1] J. Jing *et al.*, "Recent advances on image edge detection: A comprehensive review," *Neurocomputing*, vol. 503, pp. 259-271, 2022.

[2] X. Soria *et al.*, "Dense extreme inception network for edge detection," *Pattern Recognition*, vol. 139, 109461, 2023.

[3] T. Liu *et al.*, "Edge detection imaging by quasi-bound states in the continuum," *Nano Letters*, vol. 24, (45), pp. 14466-14474, 2024.

[4] N. You *et al.*, "Research on image denoising in edge detection based on wavelet transform," *Applied Sciences*, vol. 13, (3), 1837, 2023.

[5] D. U. Gang *et al.*, "Sub-pixel edge detection method based on canny-franklin moments," *Computer Integrated Manufacturing System*, vol. 31, (3), 903, 2025.

[6] J. Guo, Y. Yang, and X. Chen, "Research on sub-pixel accuracy flange disk dimension measurement based on machine vision," *Signal, Image and Video Processing*, vol. 18, (8): pp. 6185-6195, 2024.

[7] J. Xiong *et al.*, "Precise Z-Block positioning and dimension measurement using improved Canny edge detection and sub-pixel contour fitting," *The Journal of Supercomputing*, vol. 81, (1), 230, 2025.

[8] W. Cheng *et al.*, "A machine vision-based dimension measurement method of shaft parts with sub-pixel edge," *Measurement Science and Technology*, vol. 36, (5), 055026, 2025.

[9] G. Xu *et al.*, "A real-time model for unmarked wide-scale optical monitoring of bridge response with sub-pixel edge detection, residual correction, and transfer learning," *Structures*, vol. 86, 111235, 2026.

[10] H. Wang *et al.*, "Elevator traction wheel groove wear recognition based on lightweight YOLOv8 and sub-pixel edge detection," *Computers in Industry*, vol. 176, 104444, 2026.

[11] X. Kong *et al.*, "Full-field mode shape identification based on subpixel edge detection and tracking," *Applied sciences*, vol. 13, (2), 747, 2023.

[12] G. Shao *et al.*, "Sub-pixel convolutional neural network for image super-resolution reconstruction," *Electronics*, vol. 12, (17), 3572, 2023.

[13] H. Ruan *et al.*, "Efficient sub-pixel convolutional neural network for terahertz image super-resolution," *Optics letters*, vol. 47, (12), pp. 3115-3118, 2022.

[14] Y. Weng, Quek S T, Yeoh J K W. Robust vision-based sub-pixel level displacement measurement using a complementary strategy," *Mechanical Systems and Signal Processing*, vol. 223, 111898, 2025.

[15] Q. Zhang *et al.*, "Scaled transverse translation by planar optical elements for sub-pixel sampling and remote super-resolution imaging," *Nanophotonics*, vol. 14, (8), pp. 1203-1211, 2025.

[16] Y. C. Bai *et al.*, "Sub-pixel marking and depth-based correction methods for the elimination of voxel drifting in integral imaging display," *Optics Express*, vol. 32, (7), pp. 12243-12256, 2024.

[17] A. G. Poyraz *et al.*, "Sub-Pixel counting based diameter measurement algorithm for industrial Machine vision," *Measurement*, vol. 225, 114063, 2024.

[18] Y. Guo, C. Gong, and J. Yan, "Activated sparsely sub-pixel transformer for remote sensing image super-resolution," *Remote Sensing*, vol. 16, (11), 1895, 2024.

[19] A. G. Poyraz *et al.*, "Sub-Pixel counting based diameter measurement algorithm for industrial Machine vision," *Measurement*, vol. 225, 114063, 2024.

[20] F. Chang *et al.*, "Temporal stacking of sub-pixel offset tracking for monitoring slow-moving landslides in vegetated terrain," *Landslides*, vol. 21, (6), pp. 1255-1271, 2024.